Hydrological Processes

WILEY

SPECIAL ISSUE Hydrological Processes in Urban and Peri-Urban Landscapes of Latin America and the Caribbean: Tracer and Hydrometric Perspectives

RESEARCH ARTICLE

Hydrological Implications of Climate Change Uncertainty Propagation for Hedging-Based Reservoir Operation in Mountainous Basins

Omid Babamiri | Yagob Dinpashoh

Department of Water Engineering, University of Tabriz, Tabriz, Iran

Correspondence: Omid Babamiri (babamiri@tabrizu.ac.ir; obabamiri@yahoo.com)

Received: 19 March 2025 | **Revised:** 7 July 2026 | **Accepted:** 11 July 2026

Keywords: climate change | CMIP6 | hedging rule | hydrological response | reservoir operation | runoff uncertainty

ABSTRACT

Climate-driven uncertainty propagates through catchment hydrological response and poses a major challenge for developing robust reservoir operating policies, particularly in semi-arid mountainous basins. This study investigates how uncertainty in future climate projections influences runoff variability and, consequently, hedging-based reservoir operation under changing climate conditions. A simulation–optimization framework integrating CMIP6 climate projections, SWAT hydrological modelling, stochastic runoff generation and WEAP–MOICA optimization was developed to evaluate reservoir performance under multiple climate scenarios. Results show that runoff uncertainty is strongly seasonal, reaching its highest levels during the wet season (March–May), while its impacts on reservoir operation become most pronounced during late summer and early autumn. Under the optimised hedging policy, water-supply reliability ranges from 47% to 74%, whereas demand coverage during severe drought conditions may decline to 1.5%, accompanied by an increased risk of reservoir depletion. Compared with the Standard Operating Policy (SOP), the optimised hedging strategy substantially reduces the severity of water shortages despite lower overall reliability, indicating greater system resilience under uncertain future hydroclimatic conditions. These findings demonstrate that climate-change uncertainty propagates through hydrological response to reservoir operation and highlight the importance of explicitly incorporating hydrological uncertainty into adaptive reservoir management under future climate change.

1 | Introduction

Climate change-induced increases in temperature and precipitation variability can disrupt the hydrological cycle, leading to extreme events such as floods and droughts and altering natural surface runoff regimes (Dash et al. 2023). This is a growing threat to water users and decision-makers around the world, particularly in arid and semi-arid regions that are increasingly facing water scarcity (Gohari et al. 2017; Soltani et al. 2016). Therefore, global water managers are increasingly concerned about the potential impacts of climate change on water supply–demand dynamics. As a result, societies are expected to encounter substantial challenges in the future primarily due to water scarcity. Thus, to effectively plan and manage surface water resources, it is essential to accurately predict changes in runoff under climate change scenarios (Chen et al. 2019; Liu et al. 2021). Several studies have been conducted to investigate the impact of climate change on runoff at different watersheds. Notable examples include the works of Kamali et al. (2017), Goyal et al. (2018), Kaffas et al. (2018), Ahmadi et al. (2019), Chen et al. (2019), de Andrade et al. (2019), Xue et al. (2021), Kiprotich et al. (2021), Su et al. (2021), dos Santos et al. (2021), Chang and Su (2021), Lian et al. (2021), Lian et al. (2021) Babaeian et al. (2021) and Samavati et al. (2023). However, relatively few studies have explicitly linked climate-driven hydrological uncertainty to adaptive reservoir operation.

To mitigate the negative impacts of climate change on water resources, increasing water supply through dam construction and reservoir expansion may be necessary (Chen 2003). However, it is crucial to evaluate and potentially modify existing reservoir operation policies to ensure sustainable water management and promote global socioeconomic development (Babamiri and Marofi 2021; Chong et al. 2024). Different policies govern the operation of reservoirs and each can function in unique ways. The challenge for water resources planners is to derive the most effective operating rules from a collection of policies aimed at achieving specific objectives (Gomes et al. 2021). The operation of dam reservoirs in arid and semi-arid regions involves complex decision-making processes. In these climates, implementing hedging policies is crucial for managing water allocation over time to minimise losses due to water shortages caused by droughts (Bayazit and Ünal 1990; Draper and Lund 2004; Zeng et al. 2019). Dash et al. (2023) conducted the operation of the reservoir using the coupled SWAT and HEC-RAS models, along with a genetic algorithm under climate change using CMIP5. Their goal was to provide maximum environmental flow. There were no hedge rules used in this study.

To cope with increasing hydroclimatic variability, reservoir operating policies must become more adaptive and resilient. Among the available operating strategies, hedging policies have received considerable attention because they intentionally ration water during moderate shortages to reduce the risk of severe deficits during prolonged droughts. Several hedging rules have been suggested regarding the timing, magnitude and proportion of water rationing. The timing of hedging is usually defined by specific critical water availability levels that determine when to initiate and conclude the hedging process, such as starting water availability and ending water availability (Bayazit and Ünal 1990). A hedging factor may indicate the percentage by which water delivery is reduced (Shiau 2009). Many studies utilise trial-and-error methods to evaluate various parameters of hedging rules about reservoir operation performance (Bayazit and Ünal 1990; Shiau 2003; Shiau and Lee 2005), while others focus on optimising these parameters for different applications (Kumar and Kasthurirengan 2018; Shiau 2009; Bayesteh and Azari 2021). The majority of research has employed linear hedging, which features a constant hedging factor, including one-point or two-point hedging based on water availability conditions that trigger the start of hedging (Draper and Lund 2004; Taghian et al. 2014; Aboutalebi et al. 2015; Ji et al. 2016). The primary objective of most studies is to establish reservoir hedging rules that simultaneously minimise two conflicting shortage characteristics (Shiau and Lee 2005; Kumar and Kasthurirengan 2018). These rules are suitably parameterised to facilitate a simulation-optimization framework (Fayaed et al. 2013; Gomes et al. 2021; Zeng et al. (2019); Mansouri et al. 2024; Babamiri et al. 2026), allowing for an exploration of the trade-off between two opposing objective functions: total shortage ratio and vulnerability, which arise from long-term operations.

Although numerous studies have investigated reservoir optimization and hedging policies, considerably less attention has been paid to how climate-driven uncertainty propagates through the hydrological system and ultimately influences reservoir operating decisions. Reservoir operation is inherently affected by uncertainties originating from climate projections, catchment hydrological response and inflow variability. These uncertainties propagate through the modelling chain and directly influence the effectiveness and robustness of reservoir operating policies, particularly under future climate conditions.

Dam and reservoir systems are inherently subject to multiple sources of uncertainty arising from both natural hydrological variability and engineering constraints. Major sources of uncertainty include future water demand, reservoir inflows, climate projections and hydrological model response (Berhe et al. 2013). To address these challenges, several studies have investigated different sources of uncertainty in reservoir operation. For example, Zhao et al. (2011) evaluated forecast uncertainty in real-time reservoir operation by simulating the dynamic evolution of forecast errors. Their results demonstrated that explicitly accounting for forecast uncertainty is particularly important for reservoirs with limited storage capacity. Similarly, Muronda et al. (2021) employed the Generalized Likelihood Uncertainty Estimation (GLUE) framework together with Particle Swarm Optimization (PSO) to investigate uncertainty in optimal reservoir operation. However, their uncertainty analysis was based on stochastic inflow forecasting and did not consider climate-change-induced hydrological uncertainty or hedging-based operation. Other studies have incorporated fuzzy logic to reduce uncertainty in reservoir operation (Akter and Simonovic 2004; Gomes et al. 2021; Babamiri et al. 2022), although these studies mainly addressed operational uncertainty rather than uncertainty propagation from future climate and hydrological variability.

Among the available uncertainty analysis techniques, the GLUE framework has been widely adopted because of its conceptual simplicity, flexible assumptions and ability to quantify predictive uncertainty in hydrological systems (Beven and Binley 2014; Dai et al. 2018; Noorali et al. 2026). GLUE has been successfully applied to evaluate uncertainty in hydrological predictions using Monte Carlo sampling and Bayesian concepts (Blasone et al. 2008). Previous studies have demonstrated its effectiveness for quantifying prediction uncertainty in hydrological modelling (Li and Wu 2006; Hrachowitz et al. 2013; Zhong et al. 2022; Moshizi et al. 2023; Babamiri and Dinpashoh 2024). Nevertheless, its application to evaluating how climate-driven runoff uncertainty propagates into hedging-based reservoir operation under future climate conditions remains limited.

Despite substantial progress in climate impact assessment and reservoir optimization, an important knowledge gap remains regarding how uncertainty in future climate projections propagates through hydrological response to influence adaptive reservoir operation. Previous studies have primarily focused either on runoff simulation under climate change or on reservoir optimization using deterministic or stochastic inflows. Consequently, the effects of climate-driven runoff uncertainty on hedging-based reservoir operation remain insufficiently understood, particularly in mountainous semi-arid basins where seasonal runoff variability strongly controls water availability and reservoir performance.

Therefore, rather than simply developing a simulation–optimization framework, this study seeks to improve understanding of

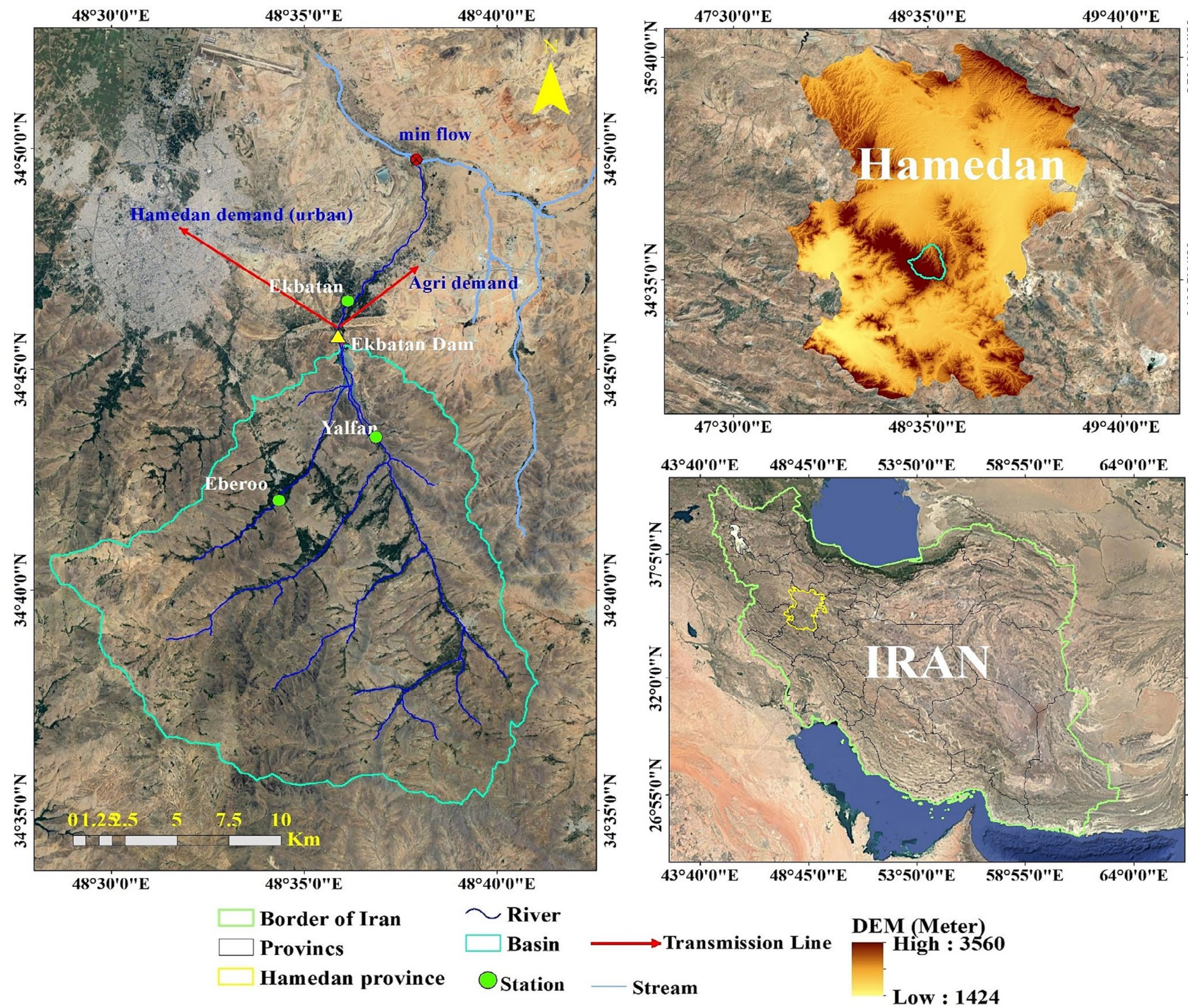

FIGURE 1 | Geographical location of Ekbatan watershed and Ekbatan Dam, Iran.

how climate-driven hydrological uncertainty propagates from runoff generation to reservoir operation under future climate conditions. Specifically, the objectives of this study are: (1) To investigate how uncertainty in CMIP6 climate projections influences future runoff variability in a mountainous semi-arid watershed, (2) to quantify how runoff uncertainty propagates into hedging-based reservoir operation under future climate conditions and (3) to evaluate the extent to which optimised hedging policies improve reservoir performance and resilience compared with the Standard Operating Policy (SOP) under uncertain hydroclimatic conditions.

These objectives were achieved using a coupled simulation–optimization framework integrating CMIP6 climate projections, SWAT hydrological modelling, stochastic runoff generation and WEAP–MOICA optimization. By explicitly linking climate uncertainty, hydrological response and adaptive reservoir operation, this study provides new insight into the propagation of climate-driven uncertainty through hydrological processes and its implications for sustainable reservoir management.

2 | Materials and Methods

2.1 | The Study Area

The sub-basin of the Central Zagros Basin in western Iran, known as the mountain watershed of Ekbatan Dam, spans from longitude 48, 28′, 13′′ to 48, 41′, 02′′ and latitude 34, 35′, 22′′ to 34, 45′, 43′′. The catchment area of Ekbatan Dam, which has an elevation range of 1970–3467 m, covers an area of 221.55 km^2. Figure 1 shows the location of Ekbatan dam watershed in Iran. The Eberoo and Yalfan rivers both converge at the Ekbatan Dam, which supplies the municipal water demands of Hamedan city and agriculture demand, as well as provides environmental flow from this reservoir. Based on the data from Hamedan synoptic station, the average precipitation, average maximum temperature and average minimum temperature in the basin are 316.73 mm, 20.2°C and 4.4°C, respectively (http://www.irimo.ir). The mean annual potential evaporation in Hamedan station is about 1350 mm per year (Dinpashoh et al. 2011). The Köppen Geiger (Kottek et al. 2006) climate classification characterises the basin's climate as semi-arid.

TABLE 1 | Characteristics of the eight CMIP6 GCMs used in this study (Babaousmail et al. 2022).

No.	Model name	Modelling centre (or group)/country	Atmospheric resolution (lon × lat)
1	ACCESS-CM2	Commonwealth Scientific and Industrial Research Organization/Australia	1.25° × 1.875°
2	CNRM-CM6-1	Centre National de Recherches Météorologiques–Centre Européen de Recherche et de Formation Avancée en Calcul Scientifique/France	1.4° × 1.4°
3	CNRM-ESM2-1		
4	INM-CM4-8	Institute for Numerical Mathematics/Russian Academy of Science/Russia	1.5° × 2°
5	INM-CM5-0		
6	MIROC6	Japan Agency for Marine-Earth Science and Technology, Atmosphere and Ocean Research Institute, The University ofTokyo, National Institute for Environmental Studies and RIKEN Center for computational Science/Japan	1.4° × 1.4°
7	MIROC-ES2L		

2.2 | Future Climate Scenarios (CMIP6 SSP Scenarios)

A new generation of GCMs developed for CMIP6 have been published by the IPCC (AR6) which is now available. These experiments are based on advanced GCMs that more accurately represent the complex physical processes within the climate system than previous GCMs (Wang et al. 2018; Siabi et al. 2023). Based on the most recent trends in anthropogenic carbon emissions, CMIP6 introduced a new projection scenario known as the rectangular combination of SSPs and RCPs (Peng and Li 2021). In general, new SSPs are scenarios that, in addition to previous RCP concepts, take into account future socio-economic changes and contribute to mitigating climate change. Nevertheless, the CMIP6 climate projections differ from the previous version (CMIP5), not only because of newer forms of climate models coupled with SSP scenarios, but also because they show new gap scenarios that were not previously covered (Siabi et al. 2023). CMIP6 contains seven scenarios: The four scenarios SSP1-2.6, SSP2-4.5, SSP4-6.0 and SSP5-8.5 are the updated RCP2.6, RCP4.5, RCP6.0 and RCP8.5 scenarios available in CMIP5 and the scenarios SSP1-1.9, SSP4-3.4, SSP3-7.0 are newly added to this project (Gupta et al. 2020). Although the historical simulations of CMIP6 cover the period 1850–2014, the current study considered the 20-year period 1990–2014 to be the baseline period and corresponded to the station period. To analyse the GHG emission scenarios in each model under different climate policies, minimum temperature, maximum temperature and precipitation from the output of 7 GCMs based on SSP1-2.6, SSP2-4.5, SSP5-8.5 for the near future period (2023–2042) were obtained from the ECMWF-COPERNICUS website at https://cds.climate.copernicus.eu/. The specifications of the GCMs used in the study and their development institutions are listed in Table 1.

2.2.1 | Bias Correction Method

A variety of methods have been developed to correct bias in the output of GCMs, ranging from simple scaling methods to more complex distribution mapping methods (Luo et al. 2018). Linear Scaling (LS) is an effective technique in this case (Yao et al. 2021). The monthly average of the corrected values is fully consistent with the observed values in the LS method. This method typically corrects precipitation with a multiplier and temperature with an additive value on a monthly basis, as demonstrated in Equations (1) and (2), respectively. The assumption is that there will be no change in the correction factors and additives in use, even under future conditions (Teutschbein and Seibert 2012; Luo et al. 2018)

$$P^{cor}_{hst,m,d} = P_{hst,m,d} \times \left[\frac{\mu(P_{obs,m})}{\mu(\mathrm{P}_{hst,m})} \right] \quad (1)$$

$$T^{\mathrm{cor}}_{hst,m,d} = T_{hst,m,d} + \left[\mu(T_{obs,m}) - \mu(T_{hst,m}) \right] \quad (2)$$

$P^{cor}_{hst\ m\ d}$ and $T^{cor}_{hst\ m\ d}$ are the corrected precipitation and temperature on the dth day of the mth month, respectively; $P_{hst,m,d}$ and $T_{hst,m,d}$ represent the precipitation and temperature resulting from the main outputs of the GCM in the respective period. The subscripts d and m denote specific days and months, respectively and μ indicates the average value.

2.3 | SWAT Model

This study uses a semi-distribution physical hydrological model known as SWAT to simulate and predict long-term runoffs, sedimentations and chemical-agricultural products in the Ekbatan watershed. The simulation of hydrological processes is done in two phases: ground or soil profile and routing (Arnold et al. 1998). The ground phase calculates the inflow of water, sediments, nutrients and pesticides to the main channel in each reservoir based on the water balance concept that considers processes such as rainfall, evapotranspiration, seepage, surface runoff, lateral flow and groundwater flow. The routing phase uses the main channel to connect all subbasins and simulates the movement of water and sediment towards the basin outlet (Cibin et al. 2010; Chen et al. 2019). Interflow in SWAT is calculated using a linear function that takes into account factors like slope length and angle, saturated conductivity, soil porosity and the amount of water stored in the saturated zone (Gebremariam et al. 2014). SWAT simulates hydrological cycles based on the water balance equation (Equation 3).

$$SW_t = SW_0 + \sum_{i=1}^{t} \left(R_{day} - Q_{surf} - E_{\mathrm{a}} - W_{\mathrm{seep}} - Q_{\mathrm{gw}}\right)_i \quad (3)$$

where SW_0 and SW_t (mm) represent the initial and final soil water content and R_{day}, Q_{surf}, E_a, W_{seep} and Q_{gw} (mm) correspond to the rainfall, runoff, evapotranspiration, interflow and base flow, respectively on the ith day, respectively.

2.3.1 | SWAT Input Data

The **s**patial **a**nalyst feature within ArcGIS software is employed by SWAT to create flow networks and basin boundaries, utilising the digital elevation model (DEM) and raster primary functions, as detailed by Abbaspour et al. (2007). Initially, the DEM10 map was acquired from the Natural Resources Department in Hamedan Province for modelling purposes, as shown in Figure 1. Since the waterway and sub-basin network was not previously delineated, it was established using the 'flow direction and accumulation' technique and subsequently examined in Google Earth, as illustrated in Figure 1. Due to the absence of a provincial soil map, a global soil map was employed and the land use map was obtained from the aforementioned unit and integrated into the GIS model.

The SWAT requires precipitation, minimum and maximum temperature, solar radiation, relative humidity and wind speed as meteorological inputs. In this study, future precipitation and temperature (2023–2042) were obtained from CMIP6 projections and used as primary drivers of runoff simulations. Due to limited availability and higher uncertainty in other climate variables, solar radiation, relative humidity and wind speed were assumed stationary and derived from historical data (2000–2020) or generated using the SWAT weather generator. This approach implies that changes in evapotranspiration are mainly driven by temperature, while other atmospheric variables remain constant, which may introduce some uncertainty in runoff estimates.

Table 2 provides an overview of the characteristics of synoptic and hydrometric stations within the Ekbatan basin. Specifically, Eberoo and Yalfan hydrometric stations are responsible for gauging runoff within the basin, while the Ekbatan Dam station, positioned at the dam's outlet, records and monitors rainfall data. Furthermore, meteorological parameters such as air temperature, radiation, wind speed and relative humidity are meticulously measured and documented at the Hamedan station, located in close proximity to the watershed.

2.4 | Water Evaluation and Planning (WEAP) Model

The WEAP model was utilised to simulate the Ekbatan Reservoir. WEAP is an advanced integrated modelling tool designed to analyse water supply, demand and environmental needs while assessing the impacts of various policies on water quantity, quality and ecosystems. It was developed by the Stockholm Environment Institute (SEI 2012). The model's core is based on mass balance equations for monthly water accounting, where total inflows are balanced with total outflows (Equation 4), adjusted for any changes in storage within reservoirs and aquifers. Each node and link in WEAP adheres to a mass balance equation, with some incorporating additional constraints on flow. For instance, inflows to a demand site cannot exceed its supply needs, aquifer outflows are limited by maximum withdrawal rates and link losses are proportional to the flow. These mass balance equations are formulated as constraints in linear programming (Muronda et al. 2021).

$$\sum (\text{Inflow}) = \sum (\text{Outflow} + \text{AdditionToStorage}) \quad (4)$$

It's also possible to change this to: Inflow–Outflow–AdditionToStorage = 0.

AdditionToStorage is applicable solely to reservoirs and aquifers. It is considered positive when there is an increase in storage and negative when there is a decrease. Outflow encompasses both consumption and losses.

2.4.1 | WEAP Input Data

The river network within the Ekbatan watershed and downstream of the dam, the location of the Ekbatan dam reservoir, hydrometric stations, water transfer canals and demand nodes (urban, agricultural and environmental) were digitised and defined in the WEAP model based on GIS base maps. Additionally, data about the reservoir's volumetric-surface-height relationships is inputted into the model for simulation purposes. The water requirements for agricultural lands, domestic consumption and the demand for environmental flow downstream of the Ekbatan Dam were calculated and used as the input into the model. The water demand for each agricultural plain was calculated based on factors such as cropping pattern, rainfall, temperature, water use efficiency and leaching requirements. Urban demands for the city of Hamedan were calculated based on demographics and per capita water consumption. The total water inflow, evaporation from the Ekbatan reservoir and total demand are presented in Figure 2. To determine the environmental flow, the Montana method, one of the hydrological

TABLE 2 | Specifications of the stations used in the present study area.

Station type	Station name	Latitude	Longitude	Elevation (m)	Data collection period
Hydrometric	Ekbatan	34°, 45′, 28″	48°, 35′, 59″	1935	2000–2020
Hydrometric	Yalfan	34°, 43′, 43″	48°, 36′, 38″	2074	2000–2020
Hydrometric	Eberoo	34°, 42′, 48″	48°, 35′, 6″	2196	2000–2020
Synoptic	Hamedan	34°, 46′, 46″	48°, 33′, 5″	1922	2000–2020

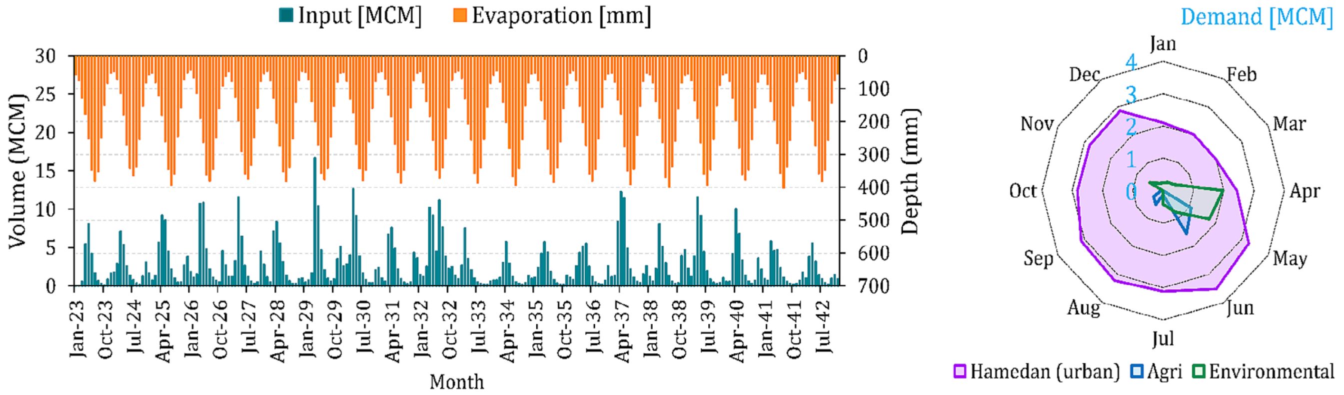

FIGURE 2 | Ensemble-based monthly reservoir inflow, evaporation losses and water demand of different users for the period 2023–2042 (radar chart).

classification methods, was used to estimate the minimum environmental flow downstream of the dam (Tennant 1976). Also, the calculation of evaporation from the dam lake was executed using the Hargreaves and Samani (1985) method.

2.5 | Multi-Objective Optimization

2.5.1 | Multi-Objective Imperialist Competition Algorithm (MOICA)

The Imperialist Competition Algorithm (ICA) is a population-based optimization method inspired by the idea of categorising countries as imperialists and colonies (Enayatifar et al. 2013). In this algorithm, each individual is represented as a country, positioned within a problem space divided into empires. The strongest country in each empire serves as the imperialist, while the remaining countries are referred to as colonies. During each iteration, termed a decade, the imperialists attract colonies towards them (Atashpaz-Gargari and Lucas 2007).

This study utilised MOICA, which focuses on finding non-dominated solutions rather than simply identifying the lowest-cost countries. The top-ranked countries form the Pareto optimal front, from which imperialists are selected to enhance solution diversity and coverage. The influence of imperialists becomes particularly significant when optimising problems with multiple objectives. In the standard ICA, a country's power is determined by its objective function, whereas in the multi-objective variant, power is evaluated across all objectives. This approach was detailed by Enayatifar et al. (2013).

2.5.2 | Objective Functions and Constraints

The MOICA algorithm aims to optimise reservoir operation by maximising the supply to downstream demands (Equation 5) while simultaneously minimising deviations from the reservoir's operating capacity (Equation 6) (Babamiri and Marofi 2021).

$$F_1 = \text{Maximise}\left(\sum_{t=1}^{n} \sum_{z=1}^{nz} \sum_{d=1}^{nd} (Cov_{tzd})\right) = \text{Minimise}\left(\sum_{t=1}^{n} \sum_{z=1}^{nz} \sum_{d=1}^{nd} \left(1 - \frac{TAW_{tzd}}{DM_{tzd}} * 100\right)\right) \tag{5}$$

where Cov_{tzd} represents the percentage of water demand met for demand site d during period t in region z; DM_{tzd} denotes the water requirement of demand site d in period t within region z; and TAW_{tzd} is the total volume of water allocated to demand site d during period t in region z.

$$F_2 = \text{Minimise}\left[\sum_{t=1}^{n}\left[\text{Max}\left(1 - \frac{S_t}{S_{min}}, 0\right)\right]\right] \tag{6}$$

where S_t represents the storage capacity of the reservoir at time step t, S_{min} denotes the minimum operating level of the reservoir and n signifies the number of simulations.

Subjected to:

$$ARS_{tzd} = \begin{cases} DM_{tzd} & \text{if}\left(TSR_t - \sum_{z=1}^{z-1} \sum_{d=1}^{d} DM_{tzd} - \sum_{z=1}^{z} \sum_{d=1}^{d-1} DM_{tzd}\right) \geq DM_{tzd} \\ \left(TSR_t - \sum_{z=1}^{z-1} \sum_{d=1}^{d} DM_{tzd} - \sum_{z=1}^{z} \sum_{d=1}^{d-1} DM_{tzd}\right) & \text{Otherwise} \end{cases} \tag{7}$$

where ARS_{tzd} represents the total surface water allocated to demand site d during period t in region z, considering the priority of the demand site; and TSR_t denotes the whole amount of water allocated in t period.

$$TDF_{tzd} = DM_{tzd} - ARS_{tzd} \tag{8}$$

$$TSW_t = SW_{DI} + SW_{Agri} + SW_{min} \tag{9}$$

$$S_{dead} \leq S_t \leq S_{max} \tag{10}$$

TDF_{tzd} represents the total deficit of demand site d in region z during period t. TSW_t represents the total water demand in period t, where SW_{DI} denotes total urban water demand, SW_{Agri} represents total agricultural water demand and SW_{min} represents total environmental water demand.

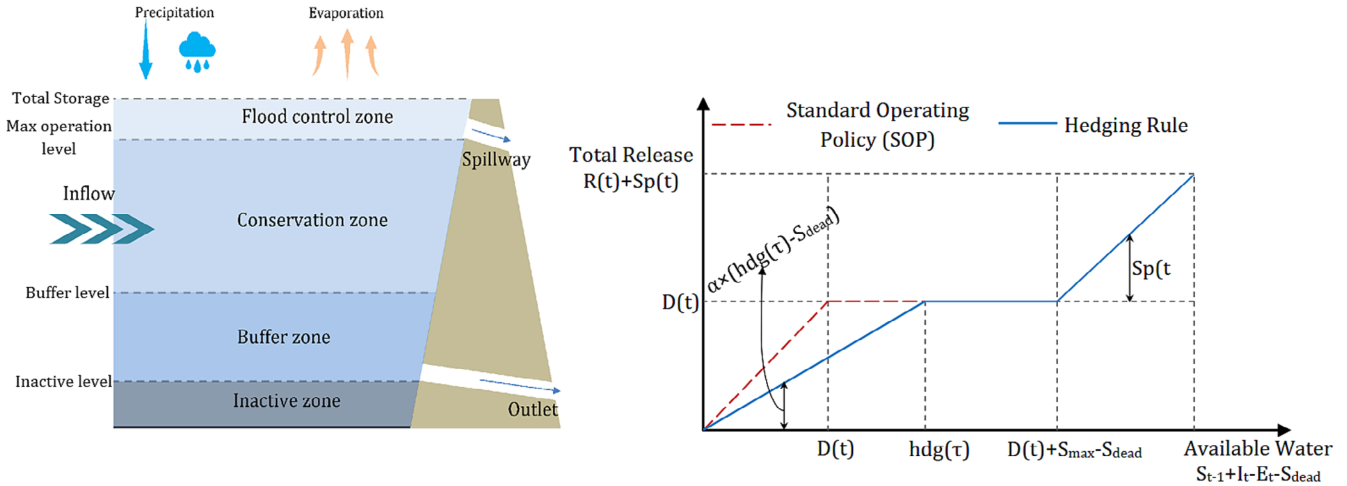

FIGURE 3 | Division of the reservoir into four zones during the operation period by the hedging method.

S_{dead} represents the dead storage volume of the reservoir, S_t denotes the reservoir volume at any given time period and S_{max} represents the maximum storage volume of the reservoir.

2.5.3 | Hedging Rule

In this study, to apply hedging rules for optimal operation, the reservoir is divided into four zones as depicted in Figure 3. According to this method, the water in the conservation zone is released freely to fully meet downstream demands. However, when the reservoir volume reaches the buffer zone, the release rate is restricted based on a hedging fraction (between zero and one) to meet downstream demands during critical conditions. The hedging parameters in this method are the reservoir storage volume [$hdg(\tau)$] and the hedging fraction (α) (Figure 3). These two parameters are generated monthly as decision variables by the optimization algorithm and the reservoir release is based on these variables in different months; therefore, the number of decision variables is 24. In other words, the determination of the buffer zone and the buffer coefficient (the fraction of downstream demand met (hedging fraction)) varies monthly and is generated using the optimization algorithm. Whenever the reservoir volume enters the buffer zone, the system (simulation–optimization framework) reduces the reservoir release based on the hedging fraction. The hedging fraction is the proportion of water in the buffer zone that is released each month. The closer this coefficient is to one, the more water is released; on the other hand, the closer it is to zero, the less water is released, meaning that the storage volume in the reservoir increases.

The general equations used for the hedging method in this study, based on Celeste and Billib (2009), are presented as follows:

Accordingly, reservoir releases occur under two distinct conditions.

The first condition is as follows:

$$\text{If: } \left[S_{t-1} - S_{dead}\right] + I_t \leq hdg(\tau) \text{ Then: } R_t = D_t \left[\frac{\left[S_{t-1} - S_{dead}\right] + I_t}{hdg(\tau)}\right] \tag{11}$$

where S_{t-1} denotes the reservoir storage at the previous time step; S_{dead} represents the dead storage (inactive storage zone) of the reservoir; I_t is the reservoir inflow at time step t; $hdg(\tau)$ denotes the hedging storage level (buffer zone) for month τ; R_t is the reservoir release; and D_t represents the downstream water demand.

The first condition is as follows:

$$\text{If: } \left[S_{t-1} - S_{dead}\right] + I_t > hdg(\tau) \text{ Then: } R_t = D_t \tag{12}$$

Let S_{HDG} denote the reservoir storage at the hedging threshold, S_{max} the maximum storage capacity and S_t the reservoir storage at time step t. Under these conditions, the system can be described by the following operational states:

1. If $S_{HDG} < S_t < S_{max}$, all water demands are fully satisfied. In this condition, the combined volume of reservoir storage and inflow during time step t is sufficient to meet downstream demands; therefore, no shortage or spill occurs.
2. If $S_t > S_{max}$, spill occurs due to capacity limitations. Since storage cannot exceed S_{max}, the excess volume $\left(S_t S_{max}\right)$ is released as overflow. Despite this, all downstream demands are still fully met, similar to the previous case.
3. If $S_t < S_{HDG}$, reservoir releases are governed by hedging rules. According to Equation (11) and the defined hedging policy, only a fraction of the total demand is supplied in order to conserve storage. In this state, shortages occur, but no overflow is expected.
4. If $S_t \leq S_{min}$, the reservoir reaches its minimum (inactive) storage level. This situation typically arises under severe drought conditions. The storage is effectively limited to S_{min} and the reservoir is unable to adequately meet downstream water demands; in extreme cases, no water can be allocated.

The implementation of the hedging approach in this study can be described as follows. Within the coupled WEAP–MOICA framework, the optimization algorithm (MOICA) is configured to generate 24 decision variables. Specifically, 12 variables correspond to monthly buffer storage levels and the remaining 12 represent the monthly demand satisfaction ratios for downstream water requirements. It should be noted that the buffer storage level in the WEAP model is equivalent to the hedging threshold, that is, the reservoir storage level at which hedging is initiated. These 24 decision variables are subsequently incorporated into the WEAP model. The first set of 12 variables defines the monthly hedging storage levels (buffer zone), with each value assigned to a specific month of the year. The second set of 12 variables specifies the percentage of downstream demand to be satisfied in each month. The WEAP model is then executed based on these decision variables, which effectively determine the hedging policy through buffer storage coefficients and demand allocation ratios. This iterative process, consisting of decision variable generation by MOICA and simulation by WEAP, continues until convergence to the Pareto optimal front is achieved. Ultimately, the optimal set of monthly decision variables is obtained, based on which reservoir release policies are determined.

2.5.4 | MOICA Parameter Settings

The optimal ICA parameters for this study are summarised in Table 3. The revolution rate is heavily influenced by the size of the solution space and a value of 0.2 was deemed appropriate for this case. The direction parameter (β) dictates the extent to which a colony aligns with its imperialist during the assimilation process; when $\beta > 1$, colonies approach the imperialist from both sides. In this study, a value of 2 was selected for β. The deviation parameter (θ) is critical in ICA as it balances exploration (introducing randomness to diversify the search) and exploitation (intensifying the search with more focus). Literature (Babamiri and Dinpashoh 2024) suggests that setting θ to $\pi/4$ strikes a balance between accuracy and search efficiency, making it a suitable choice for most cases. The parameter ζ, which represents the average power of colonies in each empire and is a positive constant, was set to 0.1 for this study, based on literature recommendations favouring small values such as 0.1 or 0.15.

2.6 | Performance Evaluation Criteria

To evaluate the performance of the reservoir operation policies, two indices including reliability and coverage were employed.

Reliability represents the fraction of time periods during which the system fully satisfies the downstream demand:

TABLE 3 | Optimised parameters to run MOICA.

Parameter	Value
The number of initial countries	48
Number of Initial Imperialists	4
Revolution rate	0.2
β	2
θ	$\pi/4$
ζ	0.1

$$Rel = \frac{1}{N} \sum_{t=1}^{N} I_t \text{ where } I_t = \begin{cases} 1 & \text{if } R_t \geq D_t \\ 0 & \text{if } R_t < D_t \end{cases} \tag{13}$$

where N is the total number of time periods, R_t is the release at time step t, D_t is the demand at time step t, *and* I_t is an indicator function showing whether demand is fully met.

Coverage was computed at each time step (monthly) as follows:

$$Cov = \frac{min(R_t, D_t)}{D_t} \tag{14}$$

where R_t is the release at time step t and D_t is the demand at time step t.

2.7 | Uncertainty Analysis Based on Likelihood-Based Ensemble Approach (GLUE Inspired)

In this study, an ensemble-based uncertainty analysis framework with likelihood weighting was applied to evaluate the variability of projected runoff under a given climate scenario. This approach is inspired by the GLUE methodology, but differs from the classical parameter-based implementation. Specifically, no model parameters from SWAT were sampled. Instead, uncertainty arises from climate model variability (based on CMIP6 projections) and Monte Carlo–generated runoff time series.

First, to assess the variability of future monthly runoff under CMIP6 scenarios using the SWAT model, runoff was first simulated for all selected climate models. Subsequently, stochastic time series generation was performed based on an ensemble-driven Monte Carlo approach. Specifically, for each scenario (e.g., SSP1-2.6), seven monthly runoff time series were obtained from different climate models over the future period (2023–2042), each consisting of 240 monthly values. Thus, for each month, seven alternative runoff values were available. A new synthetic time series was generated by randomly selecting one value from these seven candidates for each month. This random sampling procedure was repeated 30 times, resulting in 30 stochastic runoff series per scenario. The key advantage of this approach is that it preserves inter-model variability and associated uncertainty. This procedure was applied to all three scenarios, yielding a total of 90 stochastic monthly runoff time series for the basin over the period 2023–2042. Each time series therefore contains 20 values for each calendar month (e.g., 20 January values per series). Across the 90 simulated series, this results in 90 sets of 20 values for each month of the year.

To evaluate the consistency of simulated runoff with historical conditions, a likelihood measure was computed separately for each month. The observational reference was defined using historical climatology derived from the period 2004–2023. For each month, the observed mean (μ) and standard deviation (σ) were calculated from 20 historical values (e.g., 20 observed January runoff values).

The likelihood value (L_i) for each simulated series i was computed using a Gaussian likelihood function:

$$L_i = \exp\left(- \frac{\left(Q_{sim,i} - \mu\right)^2}{2\sigma^2} \right) \tag{15}$$

where $Q_{sim,i}$ represents the runoff series generated using Monte Carlo (or aggregated monthly statistic) for series i and μ and σ denote the historical monthly (2000–2020) mean and standard deviation, respectively.

For each month, this procedure yields 30 likelihood values corresponding to the 30 simulated runoff series. These likelihood values were then normalised to obtain weights (P_i):

$$P_i = \frac{\boldsymbol{L_i}}{\sum_{\boldsymbol{i=1}}^{\boldsymbol{30}} \boldsymbol{L_i}} \tag{16}$$

Using an acceptable threshold (ASR), simulations that result in better agreement with historical climatology (i.e., higher likelihood values) were distinguished from the rest. Specifically, likelihood values (L_i) were sorted in descending order and a subset of top-performing simulations was selected as the acceptable set. In this study, the acceptable threshold was defined as 1% of the total number of samples (n), following recommendations from previous studies applying GLUE-based approaches (Babamiri and Dinpashoh 2024; Muronda et al. 2021).

These likelihood-based weights and/or the selected acceptable simulations were then used to derive uncertainty bounds for each month, either through weighted statistics or percentile-based ranges. This approach allows for incorporating both inter-model variability and stochastic variability while maintaining consistency with observed climatological patterns.

It is important to note that this framework represents a likelihood-based ensemble evaluation approach rather than a classical GLUE application, as no parameter sampling or prior parameter distributions were considered.

2.8 | Coupled Simulation–Optimization Procedure

The proposed framework integrates climate projections, hydrological modelling, stochastic runoff generation, reservoir simulation and multi-objective optimization. First, bias-corrected precipitation and temperature projections from seven CMIP6 climate models under three SSP scenarios were used to drive the calibrated SWAT model, producing 21 runoff time series (seven for each SSP scenario) for the period 2023–2042. The runoff series were then grouped according to the three SSP scenarios and 30 stochastic runoff series were generated from each group using the Monte Carlo method, resulting in a total of 90 runoff time series.

The calibrated WEAP model was coupled with the Multi-objective Imperialist Competitive Algorithm (MOICA) through a custom VBScript developed in MATLAB. For each of the 90 stochastic runoff series, an independent simulation–optimization run was performed to derive the optimal hedging policy. Consequently, 90 Pareto fronts were obtained, from which the preferred operating policies were selected. Monthly demand coverage was subsequently calculated and the uncertainty bounds of reservoir performance were derived from the ensemble of the 90 optimised simulations. The optimization parameters and stopping criteria remained unchanged for all runs and are presented in Sections 2.5.4 and 3.5.

3 | Results

3.1 | Evaluating the Selected CMIP6 Models

Figure 4 presents Taylor diagrams comparing the performance of the selected CMIP6 models before and after bias correction for precipitation, maximum temperature (Tmax) and minimum temperature (Tmin) over the baseline period (1995–2014). Prior to bias correction, the MIROC-ES2L model exhibited the best performance for precipitation, with an RMSE of 10.3 mm/month and a correlation coefficient (R) of 0.88, as indicated by its proximity to the observational reference point. For Tmax, both MIROC-ES2L and ACCESS-CM2 showed superior performance, with high correlation values ($R \approx 0.99$) and relatively low RMSE values (1.97 and 1.98, respectively). Similarly, for Tmin, the MIROC-ES2L model achieved the lowest error among the evaluated models (RMSE = 2.1, $R = 0.98$). Following bias correction, all models demonstrated substantial improvements, with reduced errors and increased agreement with observations. The corrected outputs closely matched the observed data across all variables, indicating that the bias correction procedure effectively enhanced the reliability of the climate model simulations.

3.2 | Evaluating of SWAT Model

The statistical performance of the SWAT model during the calibration (2004–2016) and validation (2017–2020) periods is summarised in Table 4. Overall, the model reproduced the observed monthly runoff satisfactorily at both the Yalfan and Eberoo hydrometric stations. The coefficient of determination (R^2) ranged from 0.67 to 0.73, while the Nash–Sutcliffe Efficiency (NSE) varied between 0.56 and 0.72. The normalised root mean square error (NRMSE) ranged from 11.98% to 18.78% during the calibration and validation periods. The slightly lower performance during validation reflects the increased variability of observed runoff but remains within the acceptable range for hydrological modelling. Overall, the statistical indicators demonstrate that the SWAT model provides reliable runoff simulations and is therefore suitable for subsequent climate change impact assessment and reservoir operation analyses.

3.3 | Uncertainty Analysis

The changes were visualised through monthly violin plots (Figure 5). As depicted in the figure, the basin runoff exhibits a seasonal periodic trend. Notably, despite minimal precipitation from July to September, runoff persists due to the mountainous terrain and snowpack in it. The most significant potential changes in runoff occur in April and May, typically ranging between 0 and 9.59 m^3/s. The dominant distribution of

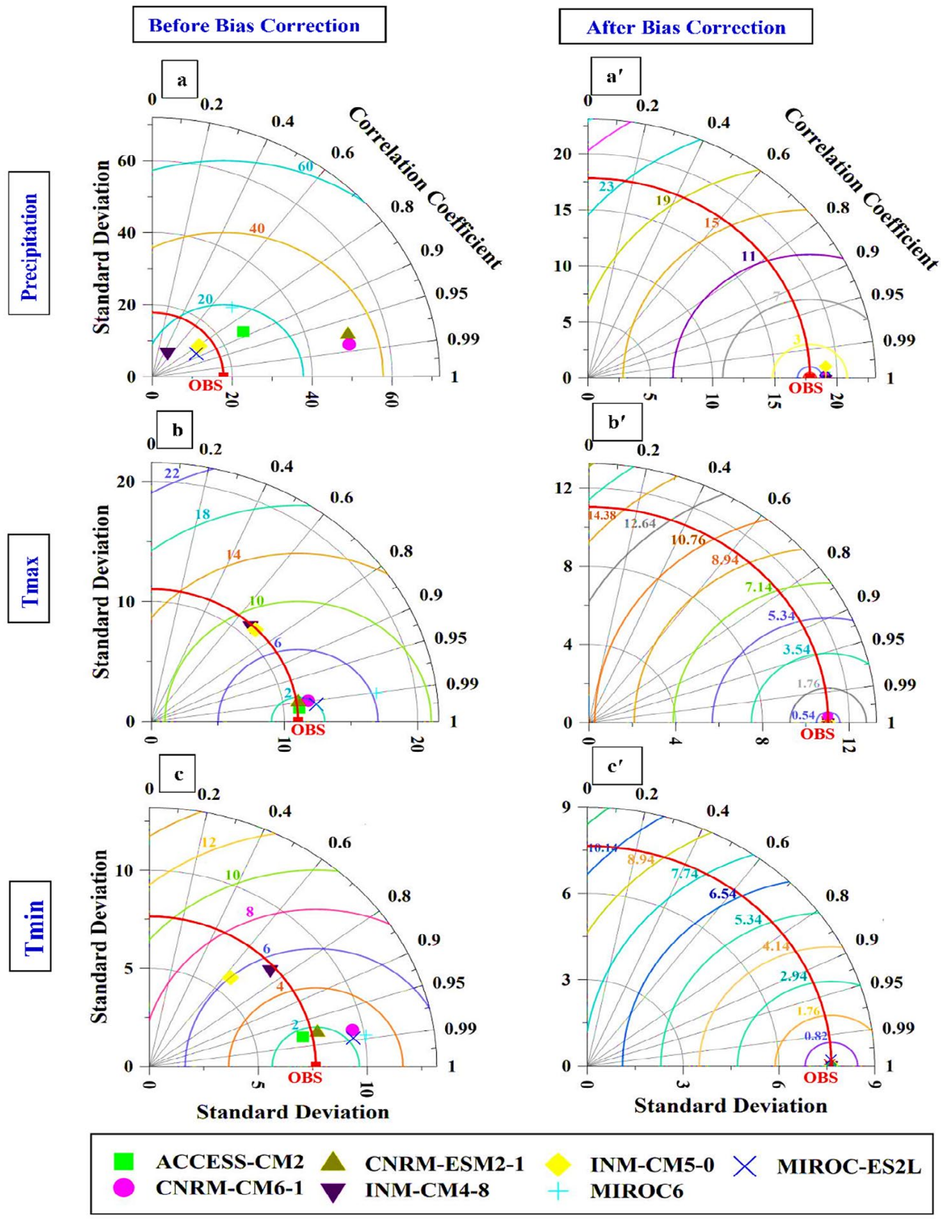

FIGURE 4 | Taylor diagrams comparing the performance of selected CMIP6 models for precipitation (upper panel), Tmax (middle panel) and Tmin (bottom panel) over the baseline period 1995–2014.

TABLE 4 | Statistical performance of the SWAT model during the calibration (2004–2016) and validation (2017–2020) periods at the Yalfan and Eberoo hydrometric stations.

	Yalfan		Eberoo	
Performance metric	**Calibration**	**Validation**	**Calibration**	**Validation**
R^2	0.73	0.68	0.67	0.75
NS	0.72	0.56	0.66	0.65
PBIAS	13.41	37.22	2.02	31.02
RMSE	0.68	1.28	0.10	0.20
NRMSE	13.39	17.79	11.98	18.78

runoff during these months lies within the 0–3.62 m^3/s range. Specifically, in April, which experiences the highest runoff levels, the interquartile range falls between 1.72 and 3.83 m^3/s.

Figure 6 illustrates the probability scatter plots (likelihood weights) of the stochastic monthly outputs, computed using Equation (16). Each point in the figure represents an

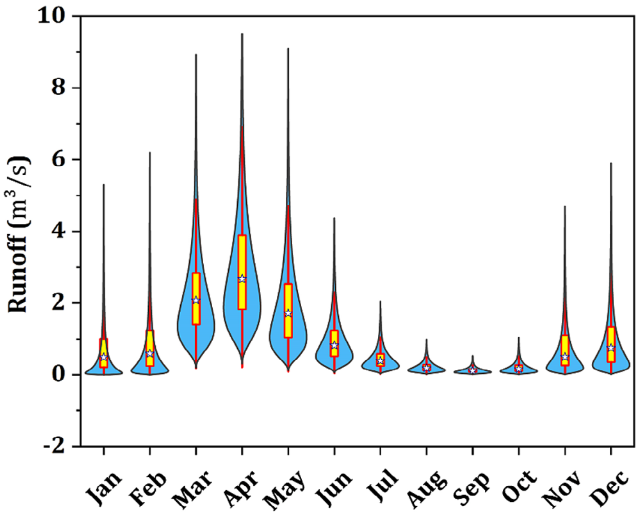

FIGURE 5 | Violin plots illustrating the uncertainty in monthly runoff based on 90 ensemble-derived stochastic time series (Monte Carlo simulation) for the Ekbatan watershed during 2023–2042.

individual likelihood value. The spread and shape of the distribution for each month reflect the degree of uncertainty: a wider and more dispersed distribution indicates higher uncertainty, whereas a more concentrated and sharply peaked distribution suggests lower uncertainty. Accordingly, the highest levels of uncertainty are observed during April, May and June, with April exhibiting the greatest variability, ranging from 0.6 to 5 m^3/s. In contrast, the lowest uncertainty is observed in October.

3.4 | WEAP Model Evaluation

The WEAP model was calibrated (2004–2016) and validated (2017–2020) and its performance is summarised in Table 5. The model achieved NRMSE values of 3.5% and 3.7% during the calibration and validation periods, respectively, while the coefficient of determination (R^2) remained 0.99 in both periods. These results demonstrate that the calibrated WEAP model provides a reliable basis for the subsequent simulation–optimization analyses.

3.5 | Results of the Stochastic Implementation of the Simulation–Optimization Framework

The MOICA algorithm was employed for the optimization process, utilising a multi-objective function to optimise 24 decision variables (hdg(τ) and α). Multiple runs of the model revealed that the initial number of countries should be at least twice the number of decision variables, leading to 48 initial countries and 8 initial imperialists. The model runs revealed significant variations in objective functions during the initial iterations. Each time series required around 400 iterations to converge to the optimal solution with the highest accuracy. The best solutions at each iteration were selected based on the objective function evaluation and stored as an optimal archive for the next stage. The Pareto front was obtained at the final iteration between the optimization objectives.

3.5.1 | Uncertainty of Pareto Fronts

Figure 7 presents the uncertainty envelope of the Pareto solutions obtained from 90 independent WEAP–MOICA simulation–optimization runs using stochastic runoff series under hedging-based operation. The values of the first and second objective functions range from 40.2 to 80.9 and from 0 to 56.1, respectively. The scatter points correspond to the Pareto solutions obtained using the two representative CMIP6 models (MIROC-ES2L and ACCESS-CM2). Each optimization run generated 50 Pareto solutions, from which the preferred operating policy was selected using the best compromise solution approach. The uncertainty envelope shown in Figure 7 represents the range of these selected solutions across all stochastic simulations.

3.5.2 | Uncertainty in Demand Coverage and Reservoir Storage

Figure 8 presents the projected uncertainty in (a) monthly demand coverage and (b) reservoir storage for the period 2023–2042. The uncertainty bands were derived from the best compromise solutions selected from the Pareto fronts obtained through 90 independent WEAP–MOICA simulation–optimization runs using stochastic runoff series. For comparison, the results corresponding to the two best-performing climate models (MIROC-ES2L and ACCESS-CM2) are also shown.

As shown in Figure 8a, the greatest uncertainty in demand coverage occurs during August and September of 2025, 2035, 2036, 2039 and 2041, when the projected coverage ranges from approximately 1.5% to 100%, indicating substantial variability in the ability to satisfy water demand. In contrast, demand coverage remains consistently close to 100% during February 2031–November 2032, April 2033–May 2034 and April 2037–May 2038, where the uncertainty band becomes negligible.

Figure 8b illustrates the corresponding uncertainty in reservoir storage. The results indicate a potential risk of reservoir overflow during April of 2023, 2028, 2029 and 2041, as well as during May and June of 2023 and 2028. Conversely, reservoir storage may decline to the inactive storage level during October 2023–October 2025, January–March 2036, October 2036–February 2037 and October 2039. The widest uncertainty intervals occur between April 2028 and July 2029 and between February and October 2036, reflecting the highest variability in projected reservoir storage under future climate conditions.

Figure 9 shows the distribution of demand reliability for the urban, agricultural and environmental demand sites during the period 2023–2042. The box plots summarise the uncertainty derived from the optimised reservoir operating policies obtained from the stochastic simulations. Urban water supply exhibits the lowest reliability, ranging from 47% to 74%, with an interquartile range of 57.5%–64.5%. In comparison, agricultural demand shows an interquartile range of 86.5%–92.2%, while environmental demand ranges from 85.0% to 94.5%. The results also indicate that agricultural and environmental demands may occasionally experience complete supply failure under the most adverse hydroclimatic conditions.

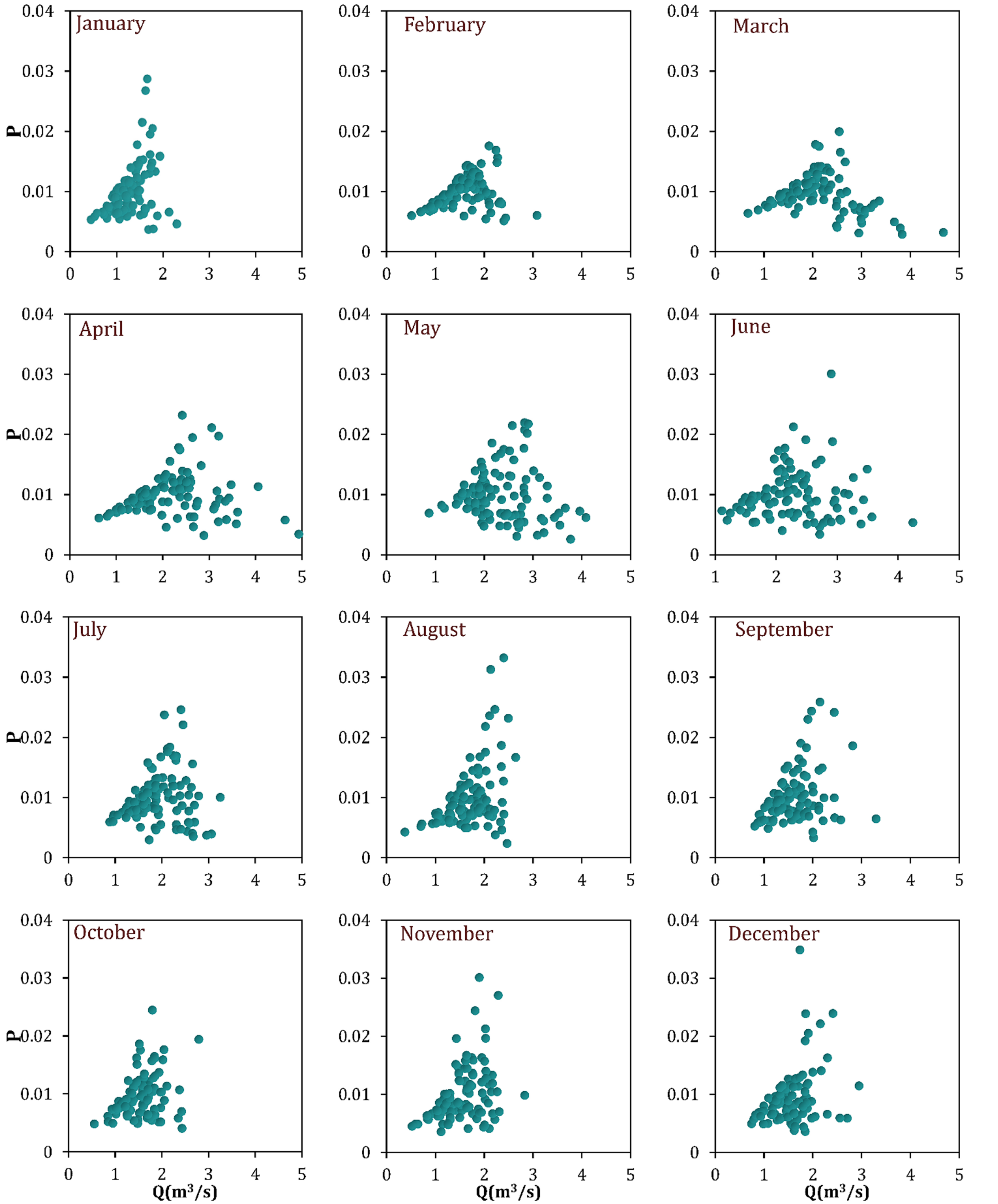

FIGURE 6 | Scatter plots of monthly runoff likelihood (P) derived from a likelihood-based ensemble framework (GLUE-inspired) using 90 stochastic time series for the period 2023–2042.

TABLE 5 | Error metric values for calibration and validation of WEAP model.

	Calibration	Validation
RMSE	0.07	0.75
NRMSE%	3.5	3.7
R^2	0.99	0.99

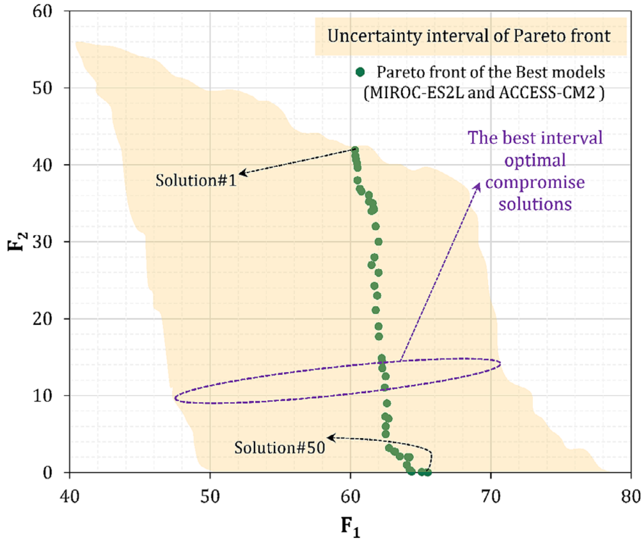

FIGURE 7 | Uncertainty band of the Pareto front (F1 versus F2) obtained from 90 stochastic runoff simulations for the period 2023–2042. F1: demand coverage objective; F2: shortage penalty objective.

3.5.3 | Comparison of Hedging Policy and Standard Operating Policy

Figure 10 compares projected demand coverage under the optimised hedging policy (Figure 10a) and the Standard Operating Policy (SOP) (Figure 10b) for the selected CMIP6 projections (MIROC-ES2L and ACCESS-CM2 under SSP2-4.5) during 2023–2042. Under the hedging policy, demand coverage remains relatively more stable over time, although considerable shortages still occur during prolonged drought periods. The most pronounced deficits are observed between November 2034 and March 2037 and again from February to October 2039, with the minimum demand coverage declining to approximately 3%–7% during August–October 2039.

The SOP exhibits substantially greater temporal variability and more severe shortages than the hedging policy. Extended periods of demand satisfaction below 50% occur between November 2034 and March 2035, August 2035 and March 2036, July 2036 and March 2037 and April to October 2039. The minimum demand coverage under SOP decreases to approximately 2.2% in September 2035, whereas the corresponding value under the hedging policy is higher (approximately 4.5%), indicating a reduction in shortage severity.

Overall, the comparison demonstrates that the hedging policy distributes water shortages more gradually through time rather than allowing complete demand satisfaction during early periods followed by severe failures after reservoir depletion. Consequently, although occasional shortages remain unavoidable under future climate uncertainty, hedging operation improves the temporal resilience of reservoir operation compared with the conventional SOP.

4 | Discussion

4.1 | Climate-Driven Hydrological Uncertainty

The results demonstrate that uncertainty associated with future climate projections is not uniformly distributed throughout the hydrological year. The largest uncertainty occurs during the wet season, particularly in April and May, when snowmelt and seasonal precipitation jointly control runoff generation in the mountainous basin. This indicates that climate-driven uncertainty primarily affects periods dominated by hydrological response processes rather than low-flow periods. Similar behaviour has been reported in previous studies conducted in mountainous catchments, where uncertainties associated with climate projections become amplified during high-flow seasons because runoff generation is highly sensitive to both precipitation variability and temperature-driven snowmelt processes (Samavati et al. 2023; Zakizadeh et al. 2021).

Among the evaluated CMIP6 climate models, MIROC-ES2L consistently provided the most reliable representation of future precipitation for the Ekbatan watershed. Similar conclusions have been reported for mountainous basins in western Iran, where the MIROC family demonstrated superior performance in reproducing regional hydroclimatic conditions (Shoja and Shamsipour 2023). Although climate model performance is inherently region-dependent, these consistent findings suggest that MIROC-based projections provide a robust basis for evaluating future hydrological responses in semi-arid mountainous catchments. This is particularly important because reliable climate projections directly influence runoff simulation and, consequently, reservoir operation under future climate conditions.

4.2 | Propagation of Uncertainty Through the Hydrological System

One of the principal findings of this study is that climate-driven uncertainty is progressively amplified as it propagates through the hydrological system, ultimately exerting a much greater influence on reservoir operation than is apparent from climate projections alone. This demonstrates that evaluating uncertainty solely at the climate or runoff stage may underestimate its consequences for water resources management, particularly in reservoir systems operating under prolonged drought conditions.

The results further indicate that runoff uncertainty generated during the wet season has disproportionately large impacts on water availability during subsequent dry months, when reservoir storage becomes the primary control on downstream water supply. Consequently, relatively small differences in projected

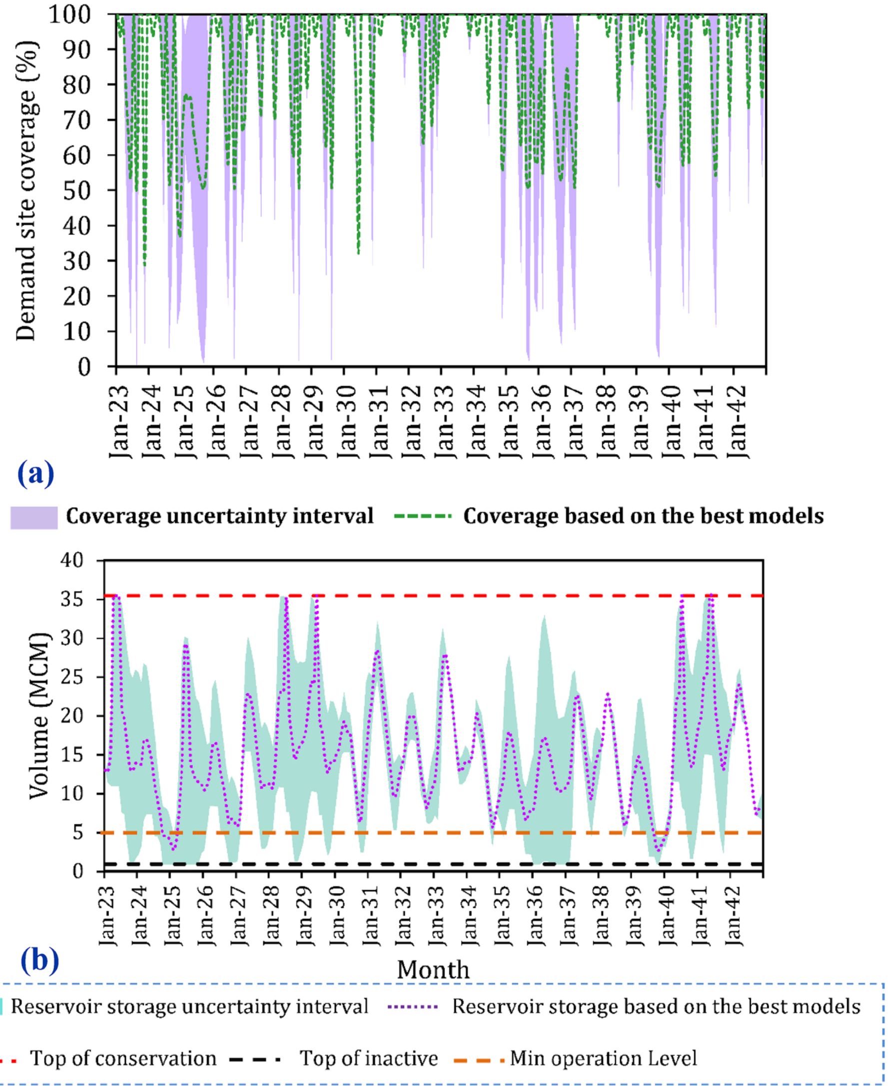

FIGURE 8 | Projected uncertainty bands of (a) monthly demand coverage and (b) reservoir storage for the period 2023–2042.

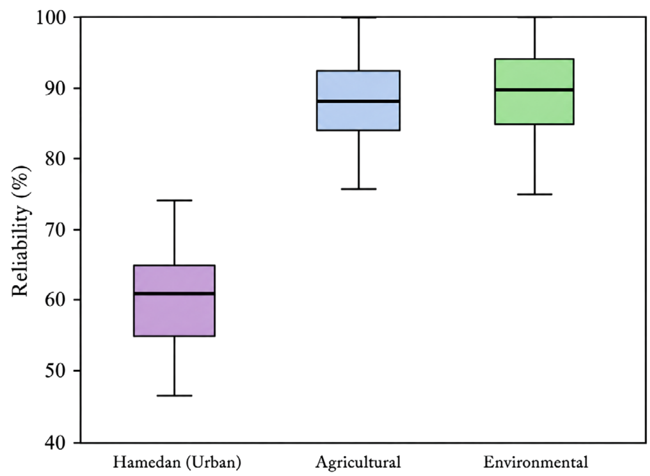

FIGURE 9 | Box plots of projected demand reliability for urban, agricultural and environmental demand sites during 2023–2042.

runoff can translate into substantial differences in reservoir storage, demand satisfaction and operational reliability. These findings highlight the importance of explicitly incorporating uncertainty into reservoir operation, rather than relying on deterministic inflow projections and provide new insight into how hydrological uncertainty influences the resilience of adaptive operating policies under future climate change.

4.3 | Hedging Improves the Temporal Resilience of Reservoir Operation

The comparison between the optimised hedging policy and the Standard Operating Policy (SOP) demonstrates that the principal benefit of hedging is not necessarily increasing reliability, but reducing the severity of water shortages during prolonged droughts. Although the reliability index under SOP is numerically higher, this metric does not fully represent operational performance because any month with demand satisfaction below 100% is classified as a failure. Consequently, months with 99% demand satisfaction contribute equally to the reliability metric as months with complete supply failure.

Instead, the hedging policy intentionally redistributes water shortages over time by introducing moderate reductions in water

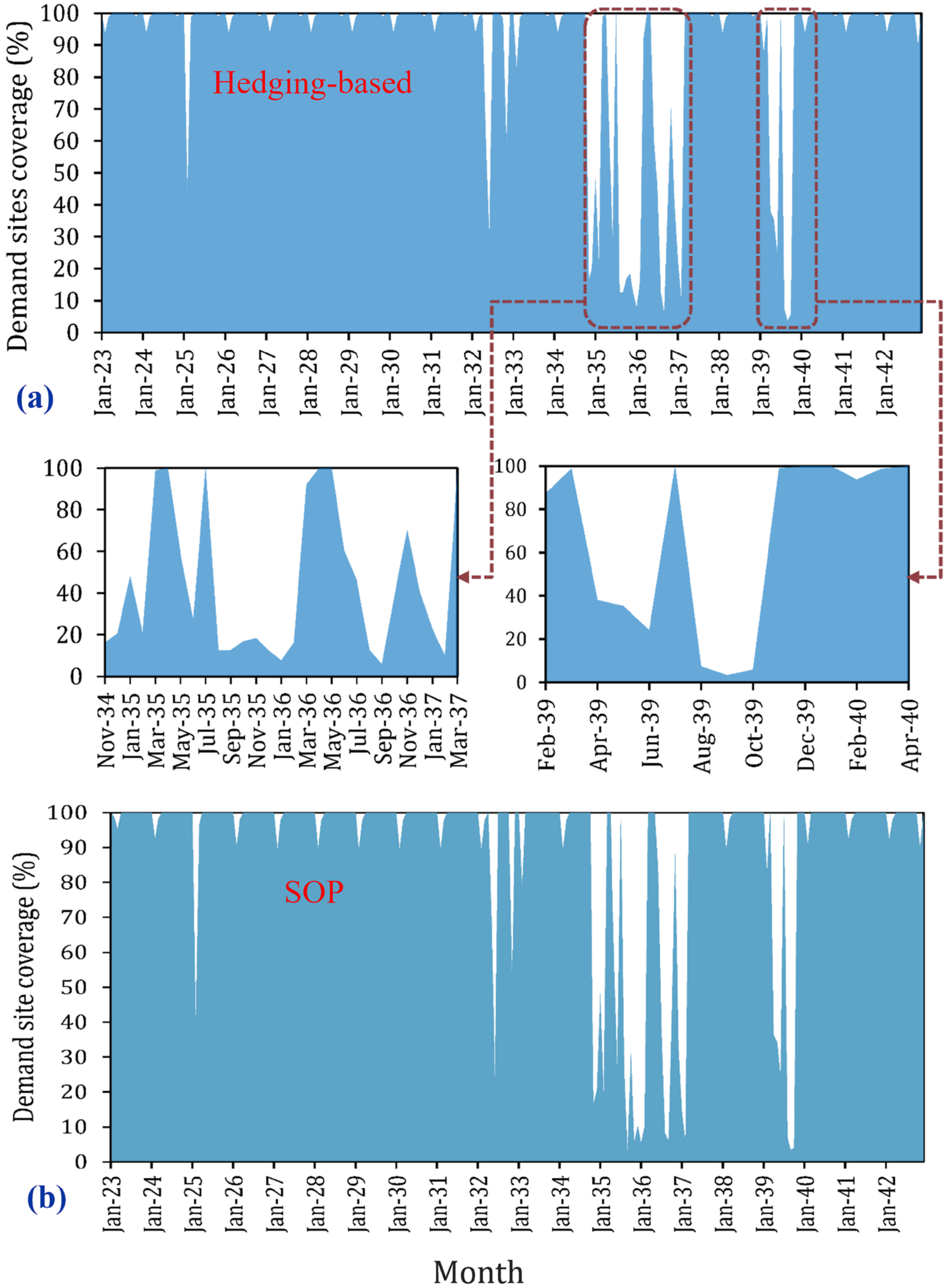

FIGURE 10 | Comparison of projected demand coverage under (a) the optimised hedging policy and (b) the Standard Operating Policy (SOP) for the selected CMIP6 projections (MIROC-ES2L and ACCESS-CM2, SSP2-4.5) during 2023–2042.

allocation before reservoir storage reaches critically low levels. This strategy substantially reduces the occurrence of severe shortages during extended droughts and enhances the temporal resilience of reservoir operation. Similar conclusions have been reported in previous hedging studies, which demonstrated that anticipatory water allocation generally outperforms conventional operating policies under prolonged drought conditions (Bayazit and Ünal 1990; Draper and Lund 2004; Shiau 2009; Gomes et al. 2021).

4.4 | Implications for Adaptive Reservoir Management Under Climate Change

The uncertainty intervals presented in this study provide practical information beyond deterministic reservoir operation. Rather than producing a single estimate of future reservoir performance, the proposed framework quantifies the range within which reservoir storage and demand satisfaction are expected to vary under future climate conditions. Such information enables water managers to identify critical periods with elevated operational risk and to develop adaptive operating strategies before severe shortages occur. Similar conclusions regarding the value of uncertainty analysis for reservoir operation have been reported by Muronda et al. (2021). However, their study focused on uncertainty associated with stochastic inflow forecasting and conventional reservoir optimization, whereas the present study explicitly propagates CMIP6 climate uncertainty through hydrological modelling into hedging-based reservoir operation, thereby providing a broader assessment of future operational risk.

More broadly, the study demonstrates that reservoir operation should increasingly shift from deterministic planning towards risk-based decision-making under future climate uncertainty. Explicitly incorporating climate-driven uncertainty into reservoir optimization provides more robust operating policies that remain effective under a wide range of possible future hydroclimatic conditions. These findings are particularly relevant for mountainous semi-arid basins, where seasonal runoff variability strongly governs future water availability.

4.5 | Future Research

The present study focused on understanding how climate-driven hydrological uncertainty propagates from CMIP6 climate projections through runoff generation to hedging-based reservoir operation. While this provides a comprehensive assessment of the influence of future hydroclimatic variability on reservoir performance, additional sources of uncertainty, such as future water demand, groundwater interactions and reservoir operating assumptions, also influence long-term water resources management and warrant further investigation.

Future research should extend the proposed simulation–optimization framework by integrating surface water and groundwater models (e.g., WEAP–MODFLOW) and by incorporating multiple uncertainty sources within a unified decision-support framework. Such developments would improve the assessment of adaptive reservoir operation and enhance the resilience of water resources systems under future climate change, particularly in semi-arid mountainous basins.

5 | Conclusion

This study demonstrates that climate-driven uncertainty propagates through the hydrological system and becomes progressively amplified from climate projections to adaptive reservoir operation. Using a coupled CMIP6–SWAT–WEAP–MOICA framework with hedging rules, the study provides new insight into how hydroclimatic uncertainty influences reservoir performance in mountainous semi-arid basins.

The results show that runoff uncertainty is greatest during the wet season, particularly in April and May, when hydrological processes are most sensitive to climate variability. Although this uncertainty originates during high-flow periods, its operational consequences become most evident during subsequent dry months when reservoir storage governs downstream water supply. Comparison with the Standard Operating Policy further demonstrates that hedging-based operation substantially reduces the severity of water shortages, despite exhibiting lower reliability according to conventional reliability metrics. These findings indicate that deterministic reservoir operation may underestimate future operational risks under climate change.

Overall, the findings highlight the importance of explicitly incorporating climate-driven uncertainty into reservoir optimization and adaptive water resources management. Rather than treating uncertainty solely as a characteristic of future climate projections, this study demonstrates that its propagation through hydrological processes directly influences reservoir resilience and operational decision-making. The proposed framework therefore provides a practical basis for developing more robust and risk-informed reservoir operating policies under future climate change.

Acknowledgements

The authors are grateful to the National Elite Foundation of Iran and the University of Tabriz for providing the postdoctoral fellowship that made this research possible.

Funding

The authors have nothing to report.

Conflicts of Interest

The authors declare no conflicts of interest.

Data Availability Statement

The corresponding author can provide access to any data, models, or codes that were utilised in this study upon receiving a reasonable request.

References

Abbaspour, K. C., J. Yang, I. Maximov, et al. 2007. "Modelling Hydrology and Water Quality in the Pre-Alpine/Alpine Thur Watershed Using SWAT." *Journal of Hydrology* 333, no. 2–4: 413–430. https://doi.org/10.1016/j.jhydrol.2006.09.014.

Aboutalebi, M., O. Bozorg Haddad, and H. A. Loáiciga. 2015. "Optimal Monthly Reservoir Operation Rules for Hydropower Generation Derived With SVR-NSGAII." *Journal of Water Resources Planning and Management* 141, no. 11: 04015029. https://doi.org/10.1061/(ASCE)WR.1943-5452.0000553.

Ahmadi, M., A. Moeini, H. Ahmadi, B. Motamedvaziri, and G. R. Zehtabiyan. 2019. "Comparison of the Performance of SWAT, IHACRES and Artificial Neural Networks Models in Rainfall-Runoff Simulation (Case Study: Kan Watershed, Iran)." *Physics and Chemistry of the Earth, Parts A/B/C* 111: 65–77. https://doi.org/10.1016/j.pce.2019.05.002.

Akter, T., and S. P. Simonovic. 2004. "Modelling Uncertainties in Short-Term Reservoir Operation Using Fuzzy Sets and a Genetic Algorithm/Modélisation D'incertitudes Dans la Gestion de Barrage à Court Terme Grâce à des Ensembles Flous et à un Algorithme Génétique." *Hydrological Sciences Journal* 49, no. 6: 1081–1097. https://doi.org/10.1623/hysj.49.6.1081.55722.

Arnold, J. G., R. Srinivasan, R. S. Muttiah, and J. R. Williams. 1998. "Large Area Hydrologic Modeling and Assessment Part I: Model Development." *JAWRA Journal of the American Water Resources Association* 34, no. 1: 73–89. https://doi.org/10.1111/j.1752-1688.1998.tb05961.x.

Atashpaz-Gargari, E., and C. Lucas. 2007. "Imperialist Competitive Algorithm: An Algorithm for Optimization Inspired by Imperialistic Competition." In *2007 IEEE Congress on Evolutionary Computation*, 4661–4667. IEEE.

Babaeian, F., M. Delavar, S. Morid, and R. Srinivasan. 2021. "Robust Climate Change Adaptation Pathways in Agricultural Water Management." *Agricultural Water Management* 252: 106904. https://doi.org/10.1016/j.agwat.2021.106904.

Babamiri, O., A. Azari, and S. Marofi. 2022. "An Integrated Fuzzy Optimization and Simulation Method for Optimal Quality-Quantity Operation of a Reservoir-River System." *Water Supply* 22, no. 4: 4207–4229. https://doi.org/10.2166/ws.2022.045.

Babamiri, O., and Y. Dinpashoh. 2024. "Uncertainty Analysis of River Water Quality Based on Stochastic Optimization of Waste Load Allocation Using the Generalized Likelihood Uncertainty Estimation Method." *Water Resources Management* 38, no. 3: 967–989. https://doi.org/10.1007/s11269-023-03704-9.

Babamiri, O., and S. Marofi. 2021. "A Multi-Objective Simulation–Optimization Approach for Water Resource Planning of Reservoir–River Systems Based on a Coupled Quantity–Quality Model." *Environmental Earth Sciences* 80, no. 11: 389. https://doi.org/10.1007/s12665-021-09681-9.

Babamiri, O., A. Noorali, and S. Marofi. 2026. "Optimized Modeling of Pollution Load Allocation in a Mountainous River of Semiarid Basin Based on Bankruptcy Rules: A Case Study of the Abbas-Abad River, Iran." *Journal of Water Resources Planning and Management* 152, no. 5: 05026006. https://doi.org/10.1061/JWRMD5.WRENG-6891.

Babaousmail, H., B. Ayugi, A. Rajasekar, et al. 2022. "Projection of Extreme Temperature Events Over the Mediterranean and Sahara Using Bias-Corrected CMIP6 Models." *Atmosphere* 13, no. 5: 741. https://doi.org/10.3390/atmos13050741.

Bayazit, M., and N. E. Ünal. 1990. "Effects of Hedging on Reservoir Performance." *Water Resources Research* 26, no. 4: 713–719. https://doi.org/10.1029/WR026i004p00713.

Bayesteh, M., and A. Azari. 2021. "Stochastic Optimization of Reservoir Operation by Applying Hedging Rules." *Journal of Water Resources Planning and Management* 147, no. 2: 04020099. https://doi.org/10.1061/(ASCE)WR.1943-5452.0001312.

Berhe, F. T., A. M. Melesse, D. Hailu, and Y. Sileshi. 2013. "MODSIM-Based Water Allocation Modeling of Awash River Basin, Ethiopia." *Catena* 109: 118–128. https://doi.org/10.1016/j.catena.2013.04.007.

Beven, K., and A. Binley. 2014. "GLUE: 20 Years on." *Hydrological Processes* 28, no. 24: 5897–5918. https://doi.org/10.1002/hyp.10082.

Blasone, R. S., J. A. Vrugt, H. Madsen, D. Rosbjerg, B. A. Robinson, and G. A. Zyvoloski. 2008. "Generalized Likelihood Uncertainty Estimation (GLUE) Using Adaptive Markov Chain Monte Carlo Sampling." *Advances in Water Resources* 31, no. 4: 630–648. https://doi.org/10.1016/j.advwatres.2007.12.003.

Celeste, A. B., and M. Billib. 2009. "Evaluation of Stochastic Reservoir Operation Optimization Models." *Advances in Water Resources* 32, no. 9: 1429–1443. https://doi.org/10.1016/j.advwatres.2009.06.008.

Chang, H. S., and Q. Su. 2021. "Exploring the Coupling Relationship of Stormwater Runoff Distribution in Watershed From the Perspective of Fairness." *Urban Climate* 36: 100792. https://doi.org/10.1016/j.uclim.2021.100792.

Chen, L. 2003. "Real Coded Genetic Algorithm Optimization of Long Term Reservoir Operation 1." *JAWRA Journal of the American Water Resources Association* 39, no. 5: 1157–1165. https://doi.org/10.1111/j.1752-1688.2003.tb03699.x.

Chen, Y., C. Y. Xu, X. Chen, et al. 2019. "Uncertainty in Simulation of Land-Use Change Impacts on Catchment Runoff With Multi-Timescales Based on the Comparison of the HSPF and SWAT Models." *Journal of Hydrology* 573: 486–500. https://doi.org/10.1016/j.jhydrol.2019.03.091.

Chong, J. Y., G. L. Hooi, Q. Y. Goh, et al. 2024. "Adapting Reservoir Operations for Optimal Water Management Under Varying Climate and Demand Scenarios Using Metaheuristic Algorithms." *Ain Shams Engineering Journal* 15, no. 8: 102835. https://doi.org/10.1016/j.asej.2024.102835.

Cibin, R., K. P. Sudheer, and I. Chaubey. 2010. "Sensitivity and Identifiability of Stream Flow Generation Parameters of the SWAT Model." *Hydrological Processes: An International Journal* 24, no. 9: 1133–1148. https://doi.org/10.1002/hyp.7568.

Dai, C., X. S. Qin, Y. Chen, and H. C. Guo. 2018. "Dealing With Equality and Benefit for Water Allocation in a Lake Watershed: A Gini-Coefficient Based Stochastic Optimization Approach." *Journal of Hydrology* 561: 322–334. https://doi.org/10.1016/j.jhydrol.2018.04.012.

Dash, S. S., B. Sahoo, and N. S. Raghuwanshi. 2023. "An Integrated Reservoir Operation Framework for Enhanced Water Resources Planning." *Scientific Reports* 13, no. 1: 21720. https://doi.org/10.1038/s41598-023-49107-z.

de Andrade, C. W., S. M. Montenegro, A. A. Montenegro, J. R. D. S. Lima, R. Srinivasan, and C. A. Jones. 2019. "Soil Moisture and Discharge Modeling in a Representative Watershed in Northeastern Brazil Using SWAT." *Ecohydrology & Hydrobiology* 19, no. 2: 238–251. https://doi.org/10.1016/j.ecohyd.2018.09.002.

Dinpashoh, Y., D. Jhajharia, A. Fakheri-Fard, V. P. Singh, and E. Kahya. 2011. "Trends in Reference Crop Evapotranspiration Over Iran." *Journal of Hydrology* 399, no. 3–4: 422–433. https://doi.org/10.1016/j.jhydrol.2011.01.021.

dos Santos, J. Y. G., S. M. G. L. Montenegro, R. M. da Silva, et al. 2021. "Modeling the Impacts of Future LULC and Climate Change on Runoff and Sediment Yield in a Strategic Basin in the Caatinga/Atlantic Forest Ecotone of Brazil." *Catena* 203: 105308. https://doi.org/10.1016/j.catena.2021.105308.

Draper, A. J., and J. R. Lund. 2004. "Optimal Hedging and Carryover Storage Value." *Journal of Water Resources Planning and Management* 130, no. 1: 83–87. https://doi.org/10.1061/(ASCE)0733-9496(2004)130:1(83).

Enayatifar, R., M. Yousefi, A. H. Abdullah, and A. N. Darus. 2013. "MOICA: A Novel Multi-Objective Approach Based on Imperialist Competitive Algorithm." *Applied Mathematics and Computation* 219, no. 17: 8829–8841. https://doi.org/10.1016/j.amc.2013.03.099.

Fayaed, S. S., A. El-Shafie, and O. Jaafar. 2013. "Reservoir-System Simulation and Optimization Techniques." *Stochastic Environmental Research and Risk Assessment* 27: 1751–1772. https://doi.org/10.1007/s00477-013-0711-4.

Gebremariam, S. Y., J. F. Martin, C. DeMarchi, N. S. Bosch, R. Confesor, and S. A. Ludsin. 2014. "A Comprehensive Approach to Evaluating Watershed Models for Predicting River Flow Regimes Critical to Downstream Ecosystem Services." *Environmental Modelling & Software* 61: 121–134. https://doi.org/10.1016/j.envsoft.2014.07.004.

Gohari, A., A. Mirchi, and K. Madani. 2017. "System Dynamics Evaluation of Climate Change Adaptation Strategies for Water Resources Management in Central Iran." *Water Resources Management* 31: 1413–1434. https://doi.org/10.1007/s11269-017-1575-z.

Gomes, L. S., A. G. Maia, and J. D. F. de Medeiros. 2021. "Fuzzified Hedging Rules for a Reservoir in the Brazilian Semiarid Region." *Environmental Challenges* 4: 100125. https://doi.org/10.1016/j.envc.2021.100125.

Goyal, M. K., V. K. Panchariya, A. Sharma, and V. Singh. 2018. "Comparative Assessment of SWAT Model Performance in Two Distinct Catchments Under Various DEM Scenarios of Varying Resolution, Sources and Resampling Methods." *Water Resources Management* 32: 805–825. https://doi.org/10.1007/s11269-017-1840-1.

Gupta, V., V. Singh, and M. K. Jain. 2020. "Assessment of Precipitation Extremes in India During the 21st Century Under SSP1-1.9 Mitigation Scenarios of CMIP6 GCMs." *Journal of Hydrology* 590: 125422. https://doi.org/10.1016/j.jhydrol.2020.125422.

Hargreaves, G. H., and Z. A. Samani. 1985. "Reference Crop Evapotranspiration From Temperature." *Applied Engineering in Agriculture* 1, no. 2: 96–99. https://doi.org/10.13031/2013.26773.

Hrachowitz, M., H. H. G. Savenije, G. Blöschl, et al. 2013. "A Decade of Predictions in Ungauged Basins (PUB)—A Review." *Hydrological*

Sciences Journal 58, no. 6: 1198–1255. https://doi.org/10.1080/02626667.2013.803183.

Ji, Y., X. Lei, S. Cai, and X. Wang. 2016. "Hedging Rules for Water Supply Reservoir Based on the Model of Simulation and Optimization." *Water* 8, no. 6: 249. https://doi.org/10.3390/w8060249.

Kaffas, K., V. Hrissanthou, and S. Sevastas. 2018. "Modeling Hydromorphological Processes in a Mountainous Basin Using a Composite Mathematical Model and ArcSWAT." *Catena* 162: 108–129. https://doi.org/10.1016/j.catena.2017.11.017.

Kamali, B., D. Houshmand Kouchi, H. Yang, and K. C. Abbaspour. 2017. "Multilevel Drought Hazard Assessment Under Climate Change Scenarios in Semi-Arid Regions—A Case Study of the Karkheh River Basin in Iran." *Water* 9, no. 4: 241. https://doi.org/10.3390/w9040241.

Kiprotich, P., X. Wei, Z. Zhang, T. Ngigi, F. Qiu, and L. Wang. 2021. "Assessing the Impact of Land Use and Climate Change on Surface Runoff Response Using Gridded Observations and Swat+." *Hydrology* 8, no. 1: 48. https://doi.org/10.3390/hydrology8010048.

Kottek, M., J. Grieser, C. Beck, B. Rudolf, and F. Rubel. 2006. "World Map of the Köppen-Geiger Climate Classification Updated." *Meteorologische Zeitschrift* 15: 259–263. https://doi.org/10.1127/0941-2948/2006/0130.

Kumar, K., and S. Kasthurirengan. 2018. "Generalized Linear Two-Point Hedging Rule for Water Supply Reservoir Operation." *Journal of Water Resources Planning and Management* 144, no. 9: 04018051. https://doi.org/10.1061/(ASCE)WR.1943-5452.000096.

Li, H., and J. Wu. 2006. "Uncertainty Analysis in Ecological Studies." In *Scaling and Uncertainty Analysis in Ecology: Methods and Applications*, edited by J. Wu, K. B. Jones, H. Li, and O. L. Loucks, 45–67. Springer. https://doi.org/10.1007/1-4020-4663-4.

Lian, Y., M. Sun, J. Wang, et al. 2021. "Quantitative Impacts of Climate Change and Human Activities on the Runoff Evolution Process in the Yanhe River Basin." *Physics and Chemistry of the Earth, Parts A/B/C* 122: 102998. https://doi.org/10.1016/j.pce.2021.102998.

Liu, Z., J. D. Herman, G. Huang, T. Kadir, and H. E. Dahlke. 2021. "Identifying Climate Change Impacts on Surface Water Supply in the Southern Central Valley, California." *Science of the Total Environment* 759: 143429. https://doi.org/10.1016/j.scitotenv.2020.143429.

Luo, M., T. Liu, F. Meng, et al. 2018. "Comparing Bias Correction Methods Used in Downscaling Precipitation and Temperature From Regional Climate Models: A Case Study From the Kaidu River Basin in Western China." *Water* 10, no. 8: 1046. https://doi.org/10.3390/w10081046.

Mansouri, S., H. Fathian, A. Nikbakht Shahbazi, M. Asadi Lour, and A. Asareh. 2024. "Optimal Operation of the Dam Reservoir in Real Time Based on Generalized Structure of Group Method of Data Handling and Optimization Technique." *Applied Water Science* 14, no. 5: 1–16. https://doi.org/10.1007/s13201-024-02159-6.

Moshizi, Z. G. N., O. Bazrafshan, H. R. Etedali, Y. Esmaeilpour, and B. Collins. 2023. "Application of Inclusive Multiple Model for the Prediction of Saffron Water Footprint." *Agricultural Water Management* 277: 108125. https://doi.org/10.1016/j.agwat.2022.108125.

Muronda, M. T., S. Marofi, H. Nozari, and O. Babamiri. 2021. "Uncertainty Analysis of Reservoir Operation Based on Stochastic Optimization Approach Using the Generalized Likelihood Uncertainty Estimation Method." *Water Resources Management* 35, no. 10: 3179–3201. https://doi.org/10.1007/s11269-021-02877-5.

Noorali, A., O. Babamiri, and S. Marofi. 2026. "Uncertainty Assessment of Mountainous River Water Quality Parameters Using the Generalized Likelihood Uncertainty Estimation Method." *Hydrological Sciences Journal* 71, no. 1: 152–165. https://doi.org/10.1080/02626667.2025.2589354.

Peng, L., and Z. Li. 2021. "Ensemble Flood Risk Assessment in the Yangtze River Economic Belt Under CMIP6 SSP-RCP Scenarios." *Sustainability* 13, no. 21: 12097. https://doi.org/10.3390/su132112097.

Samavati, A., O. Babamiri, Y. Rezai, and M. Heidarimozaffar. 2023. "Investigating the Effects of Climate Change on Future Hydrological Drought in Mountainous Basins Using SWAT Model Based on CMIP5 Model." *Stochastic Environmental Research and Risk Assessment* 37, no. 3: 849–875. https://doi.org/10.1007/s00477-022-02319-7.

Shiau, J. T. 2003. "Water Release Policy Effects on the Shortage Characteristics for the Shihmen Reservoir System During Droughts." *Water Resources Management* 17: 463–480. https://doi.org/10.1023/B:WARM.0000004958.93250.8a.

Shiau, J. T. 2009. "Optimization of Reservoir Hedging Rules Using Multiobjective Genetic Algorithm." *Journal of Water Resources Planning and Management* 135, no. 5: 355–363. https://doi.org/10.1061/(ASCE)0733-9496(2009)135:5(355).

Shiau, J. T., and H. C. Lee. 2005. "Derivation of Optimal Hedging Rules for a Water-Supply Reservoir Through Compromise Programming." *Water Resources Management* 19: 111–132. https://doi.org/10.1007/s11269-005-1502-6.

Shoja, F., and A. Shamsipour. 2023. "Projection of Future Precipitation Changes in Tehran's Water Supply Watersheds." *Journal of Natural Environmental Hazards* 12, no. 36: 151–180. https://doi.org/10.22111/jneh.2022.42622.1908.

Siabi, E. K., E. A. Awafo, A. T. Kabo-bah, et al. 2023. "Assessment of Shared Socioeconomic Pathway (SSP) Climate Scenarios and Its Impacts on the Greater Accra Region." *Urban Climate* 49: 101432. https://doi.org/10.1016/j.uclim.2023.101432.

Soltani, M., P. Laux, H. Kunstmann, et al. 2016. "Assessment of Climate Variations in Temperature and Precipitation Extreme Events Over Iran." *Theoretical and Applied Climatology* 126: 775–795. https://doi.org/10.1007/s00704-015-1609-5.

Su, X., X. Li, Z. Niu, and X. Liang. 2021. "A New Complexity-Based Three-Stage Method to Comprehensively Quantify Positive/Negative Contribution Rates of Climate Change and Human Activities to Changes in Runoff in the Upper Yellow River." *Journal of Cleaner Production* 287: 125017. https://doi.org/10.1016/j.jclepro.2020.125017.

Taghian, M., D. Rosbjerg, A. Haghighi, and H. Madsen. 2014. "Optimization of Conventional Rule Curves Coupled With Hedging Rules for Reservoir Operation." *Journal of Water Resources Planning and Management* 140, no. 5: 693–698. https://doi.org/10.1061/(ASCE)WR.1943-5452.0000355.

Tennant, D. L. 1976. "Instream Flow Regimens for Fish, Wildlife, Recreation and Related Environmental Resources." *Fisheries* 1, no. 4: 6–10. https://doi.org/10.1577/1548-8446(1976)001<0006:IFRFFW>2.0.CO;2.

Teutschbein, C., and J. Seibert. 2012. "Bias Correction of Regional Climate Model Simulations for Hydrological Climate-Change Impact Studies: Review and Evaluation of Different Methods." *Journal of Hydrology* 456: 12–29. https://doi.org/10.1016/j.jhydrol.2012.05.052.

Wang, Z., R. Zhong, C. Lai, Z. Zeng, Y. Lian, and X. Bai. 2018. "Climate Change Enhances the Severity and Variability of Drought in the Pearl River Basin in South China in the 21st Century." *Agricultural and Forest Meteorology* 249: 149–162. https://doi.org/10.1016/j.agrformet.2017.12.077.

Xue, D., J. Zhou, X. Zhao, et al. 2021. "Impacts of Climate Change and Human Activities on Runoff Change in a Typical Arid Watershed, NW China." *Ecological Indicators* 121: 107013. https://doi.org/10.1016/j.ecolind.2020.107013.

Yao, Y., W. Qu, J. Lu, et al. 2021. "Responses of Hydrological Processes Under Different Shared Socioeconomic Pathway Scenarios in the Huaihe River Basin, China." *Water* 13, no. 8: 1053. https://doi.org/10.3390/w13081053.

Zakizadeh, H. R., H. Ahmadi, G. R. Zehtabiyan, A. Moeini, and A. Moghaddamnia. 2021. "Impact of Climate Change on Surface Runoff: A Case Study of the Darabad River, Northeast of Iran." *Journal of Water* *and Climate Change* 12, no. 1: 82–100. https://doi.org/10.2166/wcc.2020.089.

Zeng, X., T. Hu, X. Cai, Y. Zhou, and X. Wang. 2019. "Improved Dynamic Programming for Parallel Reservoir System Operation Optimization." *Advances in Water Resources* 131: 103373. https://doi.org/10.1016/j.advwatres.2019.07.003.

Zhao, J., X. Cai, and Z. Wang. 2011. "Optimality Conditions for a Two-Stage Reservoir Operation Problem." *Water Resources Research* 47, no. 8: 1–16. https://doi.org/10.1029/2010WR009971.

Zhong, B., Z. Wang, H. Yang, H. Xu, M. Gao, and Q. Liang. 2022. "Parameter Optimization of SWMM Model Using Integrated Morris and GLUE Methods." *Water* 15, no. 1: 149. https://doi.org/10.3390/w15010149.